Protective effects of Notoginsenoside R1 on the ferroptosis of a human non-small cell lung cancer cell line

YUEJIAO ZHANG, ZHONGSHUN MAO and YONG DIAO

College of Sanqi Medicine and Pharmacy, Wenshan University, Wenshan Zhuang and Miao Autonomous Prefecture, Yunnan 663000, P.R. China

Received May 29, 2025; Accepted October 8, 2025

DOI: 10.3892/mmr.2025.13742

Abstract. The present study investigated the effects of Notoginsenoside R1 (NG-R1) on human non-small cell lung cancer (NSCLC) A549 cells and explored its potential mechanisms. Cell viability was assessed using the MTT assay after 72 h of treatment with varying concentrations of NG-R1 (0.1, 0.2, 0.4, 0.8, 1.6 and 2 mg/ml), which inhibited A549 cell viability in a dose-dependent manner. Cell proliferation, migration and invasion were evaluated using the BeyoClick™ EdU-594 proliferation assay, wound healing assay and Matrigel®-coated Transwell invasion assay, respectively. NG-R1 at concentrations of 0.4, 0.8 and 1.6 mg/ml significantly suppressed proliferation, migration and invasion of A549 cells compared with the control. In addition, these doses of NG-R1 increased intracellular reactive oxygen species (ROS) levels as measured using the fluorescent probe 2',7'-dichlorofluorescein diacetate. Western blot analysis revealed that treatment with NG-R1 (0.4, 0.8 and 1.6 mg/ml) upregulated the expression of the ferroptosis-related protein transferrin receptor 1, and downregulated solute carrier family 7 member 11, glutathione peroxidase 4 and ferritin heavy chain 1. Collectively, these findings indicate that NG-R1 inhibited the proliferation of NSCLC A549 cells, likely through the induction of ROS accumulation and ferroptosis.

Introduction

Lung cancer remains one of the leading causes of tumor-related deaths worldwide, accounting for ~25% of global cancer fatalities (1,2). It is primarily classified into two histological types: Small cell lung cancer (SCLC) and non-SCLC (NSCLC) (3,4). NSCLC, which includes adenocarcinoma, squamous cell carcinoma and large cell lung cancer, represents ~85% of all lung cancer cases (5). Currently, chemotherapy is the first-line treatment for SCLC and stage IV NSCLC (6); however, chemotherapy often involves administering the maximum tolerated intravenous dose of the relevant drug, which can display result in marked toxicity to healthy tissues. Furthermore, despite the initial effectiveness of chemotherapy, drug resistance and toxicity notably limit its long-term clinical success (7). Despite progress in early detection and treatment strategies, the overall 5-year survival rate for lung cancer remains at <20% (8). Therefore, developing new therapeutic agents with improved efficacy and safety profiles for lung cancer treatment is of substantial importance.

Ferroptosis is an iron-dependent form of regulated cell death driven by the accumulation of lipid peroxidation products and reactive oxygen species (ROS) (9). Unlike apoptosis, a process that is characterized by notable morphological changes such as cell membrane rupture and nuclear fragmentation (10), ferroptosis is marked by iron-dependent lipid peroxidation that causes cellular damage and death. This process involves excessive ROS accumulation and the disruption of antioxidant defense systems, distinguishing it from traditional apoptotic pathways. Notably, induction of ferroptosis has emerged as a promising therapeutic strategy, particularly for malignancies resistant to conventional treatments, positioning ferroptosis as a novel approach to induce cancer cell death (11-13).

System Xc^-, composed of the subunits solute carrier family 7 member 11 (SLC7A11/xCT) and solute carrier family 3 member 2, functions as a cystine/glutamate antiporter that imports cystine into cells while exporting glutamate (14,15). Inhibition of SLC7A11 by compounds such as erastin blocks cystine uptake, leading to depletion of intracellular L-cysteine and reduced synthesis of glutathione (GSH) (16). GSH is an important cofactor for GSH peroxidase 4 (GPX4), which detoxifies lipid peroxides by converting them into non-toxic lipid alcohols (17,18). When L-cysteine is depleted, GPX4 activity is inhibited, resulting in excessive lipid peroxide accumulation and triggering ferroptosis (16). Studies have detected the upregulation of xCT in patients with NSCLC, and targeting xCT has been shown to suppress tumor growth both *in vitro* and *in vivo* (19,20).

Panax notoginseng, a member of the Araliaceae family, has been widely used as a traditional Chinese medicine for thousands of years. Notoginsenoside R1 (NG-R1), one of

Correspondence to: Miss Yuejiao Zhang, College of Sanqi Medicine and Pharmacy, Wenshan University, 66 Xuefu Road, Kaihua, Wenshan Zhuang and Miao Autonomous Prefecture, Yunnan 663000, P.R. China
E-mail: zhangyuejiao421@163.com

Key words: Notoginsenoside R1, lung cancer, reactive oxygen species, ferroptosis

the primary bioactive compounds extracted from the root of *Panax notoginseng*, exhibits diverse pharmacological activities, including cardiovascular protection (21), neuroprotection (22) and anticancer effects (23). NG-R1 has been shown to reduce the incidence of lung cancer in a urethane-induced mouse model by improving lung barrier permeability and ameliorating histopathological changes (24). Additionally, the ethanol extract of *Panax notoginseng* inhibits migration, invasion, adhesion and metastasis of colorectal cancer cells by modulating the expression of key regulatory molecules (25). Despite numerous reports on the antitumor efficacy of NGs, to the best of our knowledge, no studies have investigated NG-induced ferroptosis in tumor cells. The present study aimed to explore the effects of NG-R1 on NSCLC using the human NSCLC cell line A549.

Materials and methods

Cell line, reagents and antibodies. Human NSCLC A549 cells were obtained from Shanghai Fuheng Biotechnology Co., Ltd. (cat. no. FH0045). NG-R1 was purchased from Shanghai Macklin Biochemical Co., Ltd. (cat. no. N814983). The ROS detection kit (cat. no. S0033), YF 594 Click-iT EdU Kit (cat. no. C0078S), BCA protein concentration assay kit (cat. no. P0012S), 2',7'-dichlorofluorescein diacetate (DCFH-DA; cat. no. S1105S), RIPA lysis buffer (cat. no. P0013B) and protease-phosphatase inhibitor cocktail (cat. no. P1045) were all sourced from Beyotime Biotechnology. Primary antibodies against GPX4 (cat. no. ab125066), ferritin heavy chain 1 (FTH1) (cat. no. ab183781), transferrin receptor 1 (TfR1) (cat. no. ab214039) and SLC7A11 (cat. no. ab175186) were purchased from Abcam. GAPDH monoclonal antibody (cat. no. AF7021), secondary antibody (goat anti-rabbit IgG, HRP-conjugated; cat. no. S0001) and ECL luminescent substrate (cat. no. K002) were obtained from Affinity Biosciences. Cell culture plates including 96-well (cat. no. 3599), 24-well (cat. no. 3527) and 6-well (cat. no. 3516), as well as Matrigel® and Transwell inserts (cat. no. 3422), were purchased from Corning, Inc. Crystal Violet Staining Solution (0.1%; cat. no. G1063) was supplied by Beijing Solarbio Science & Technology Co., Ltd. Fetal bovine serum (FBS; cat. no. A5256701) and Dulbecco's modified Eagle's medium (DMEM; cat. no. 11965092) were purchased from Gibco; Thermo Fisher Scientific, Inc. Equipment used included a CO_2 incubator (model XD-101; SANYO), precision balance (model AUW-220D; Shimadzu Corporation), refrigerated centrifuge (model MicroCL 21R; Thermo Fisher Scientific, Inc.), inverted biological light microscope (model IX73; Olympus Corporation), microplate reader (model x800; Tecan Group, Ltd.), electrophoresis and protein transfer system (model 041BR121667; Bio-Rad Laboratories, Inc.), gel imaging system (model Tanon-4600, Tanon Science and Technology Co., Ltd.) and flow cytometer (CytoFLEX V2-B2-R2; Beckman Coulter, Inc.).

Cell culture. Human NSCLC A549 cells were cultured in high-glucose DMEM supplemented with 10% FBS and 100 U/ml penicillin-streptomycin at 37˚C in a humidified atmosphere containing 5% CO_2. Cells were passaged at a 1:3 ratio every 3 days upon reaching ~90% confluency. Regular mycoplasma contamination tests were performed and yielded negative results.

Cell viability test. A549 cells in the logarithmic growth phase were seeded into 96-well plates at a density of $5x10^3$ cells/well and allowed to adhere for 24 h at 37˚C. Subsequently, the cells were treated with various concentrations of NG-R1 (0, 0.1, 0.2, 0.4, 0.8, 1.6 and 2.0 mg/ml) for 72 h at 37˚C. Following treatment, 20 μl MTT solution (0.5 mg/ml) was added to each well and incubated for 4 h at 37˚C. The supernatant was then carefully removed, and 150 μl DMSO was added to each well to dissolve the formazan crystals. Plates were gently shaken for 10 min at room temperature, and absorbance (A) was measured at 570 nm using a microplate reader; cell viability was calculated using the formula: Cell viability (%)=($A_{drug\ group}/A_{blank\ control\ group}$) x100. The half-maximal inhibitory concentration (IC_{50}) was determined using the IC_{50} calculator, an online tool provided by AAT Bioquest (https://www.aatbio.com/tools/ic50-calculator).

Cell proliferation detection. A549 cells in the logarithmic growth phase were seeded into 24-well plates at a density of $2.5x10^4$ cells/well and allowed to adhere for 24 h at 37˚C. Subsequently, the cells were treated with varying concentrations of NG-R1 (0, 0.4, 0.8 and 1.6 mg/ml) for 72 h at 37˚C. Following treatment, the supernatant was discarded and 10 μM EdU solution was added to each well for a 2-h incubation at 37˚C. EdU staining was performed using the YF 594 Click-iT EdU Kit, followed by nuclear counterstaining with Hoechst 33342, according to the manufacturer's protocol, including three PBS washes before microscopic imaging. Images were captured using an inverted fluorescence microscope and subsequently analyzed with ImageJ software (version 1.53k; National Institutes of Health).

Wound healing assay. A549 cells in the logarithmic growth phase were seeded into 6-well plates at a density of $1.0x10^6$ cells/well and cultured in medium containing 10% FBS for 24 h at 37˚C to allow adhesion. Subsequently, a 10-μl pipette tip was used to create three straight scratches per well. Floating cells were removed by washing with PBS and images of the scratch area at 0 h (W_0 h) were captured using an inverted biological light microscope. Subsequently, cells were treated with different concentrations of NG-R1 (0, 0.4, 0.8 and 1.6 mg/ml) in medium containing 2% FBS and incubated for 72 h at 37˚C before images were captured again. Images were analyzed using ImageJ software and the cell migration rate was calculated using the formula: Cell migration rate (%)=[(W_0 h-W_{72} h)/W_0 h] x100.

Cell invasion detection. Serum-free high-glucose DMEM was used to dilute Matrigel basement membrane matrix at a ratio of 1:8. Then, 50 μl diluted Matrigel was added to the upper chamber of each Transwell insert and incubated at 37˚C for 1 h to allow gelation, after which any residual liquid was carefully aspirated. A549 cells were suspended in serum-free high-glucose DMEM at a density of $1x10^5$ cells/ml. A volume of 200 μl of this cell suspension was added per well to the upper chamber coated with Matrigel. The lower chamber was filled with 600 μl high-glucose DMEM containing 10% FBS and different concentrations of NG-R1 (0, 0.4, 0.8 and 1.6 mg/ml)

and the setup was incubated for 72 h at 37˚C. After incubation, non-invasive cells on the upper surface of the membrane were gently removed with a cotton swab. The invasive cells on the lower membrane surface were fixed with 4% paraformaldehyde for 15 min at room temperature, washed twice with PBS, stained with 0.1% crystal violet for 10 min at room temperature and washed twice with PBS. Once dried, images of the invaded cells were captured using an inverted biological light microscope and analyzed using ImageJ software.

Detection of intracellular ROS. A549 cells in the logarithmic growth phase were seeded into 6-well plates at a density of $5.0x10^5$ cells/well and allowed to adhere for 24 h at 37˚C. Subsequently, the cells were treated with varying concentrations of NG-R1 (0, 0.4, 0.8 and 1.6 mg/ml) for 72 h at 37˚C. The supernatant was then discarded, and 1 ml DCFH-DA probe (diluted 1:1,000 in serum-free medium) was added to each well. Cells were incubated at 37˚C for 20 min, washed twice with PBS and subsequently digested with 0.05% trypsin. The cells were collected, resuspended in PBS and analyzed by flow cytometry recording 10,000 events per sample. Subsequent data analysis was performed using FlowJo software (version 10.0; BD Biosciences) to measure DCFH-DA fluorescence intensity, which reflects intracellular ROS levels.

Detection of expression levels of ferroptosis-related proteins. A549 cells, after being treated with varying concentrations of NG-R1 (0, 0.4, 0.8 and 1.6 mg/ml) for 72 h at 37˚C, were lysed using RIPA buffer supplemented with 1% protease and phosphatase inhibitor cocktail. Protein concentrations were determined using a BCA assay kit. Subsequently, 20 μg total protein was mixed with loading buffer and denatured at 100˚C for 10 min. Proteins were then separated by SDS-PAGE on 12% gels and transferred onto PVDF membranes using the wet transfer method. Thereafter, the membranes were blocked with 5% skim milk at room temperature for 1 h and the blocked membranes were incubated with specific primary antibodies at 4˚C overnight. The primary antibodies and their dilutions were as follows: Anti-GPX4 (1:1,000), anti-FTH1 (1:1,000), anti-TfR1 (1:1,000), anti-SLC7A11 (1:1,000), and anti-GAPDH (1:5,000). Following primary antibody incubation, the membranes were incubated with an HRP-conjugated secondary antibody (1:5,000) at room temperature for 30 min. Protein bands were visualized using the aforementioned ECL kit according to the manufacturer's instructions and images were captured with the Tanon gel imaging system. Band intensities were semi-quantified with ImageJ software.

Statistical analysis. Experimental results from three independent experiments are presented as the mean ± standard deviation. All data were analyzed using GraphPad Prism 7.0 software (Dotmatics) by one-way ANOVA followed by Dunnett's multiple comparisons test, which compared all treatment groups against a single control group. P<0.05 was considered to indicate a statistically significant difference.

Results

Effect of NG-R1 on A549 cell viability. As shown in Fig. 1, NG-R1 exhibited significant dose-dependent cytotoxicity against A549 cells. The IC_{50} value for the inhibitory effect of NG-R1 was calculated to be 0.839 mg/ml. Therefore, the concentrations of 0.4, 0.8 and 1.6 mg/ml were selected for subsequent experiments.

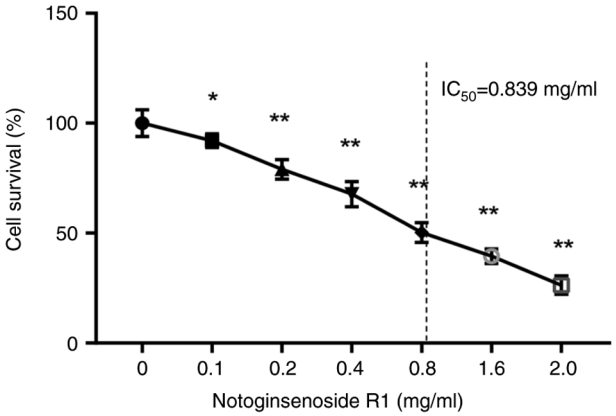

Figure 1. Effect of NG-R1 on A549 cell viability (n=6). MTT assay showed that NG-R1 inhibited the viability of A549 cells in a dose-dependent manner. The doses of NG-R1 were 0, 0.1, 0.2, 0.4, 0.8, 1.6 and 2.0 mg/ml. Data are presented as the mean ± standard deviation. The one-way ANOVA result was F (6, 35), 214.5. The dashed vertical line denotes the IC_{50}: IC_{50}, 0.839 mg/ml. *P<0.05 and **P<0.01 vs. control group. NG-R1, Notoginsenoside R1.

Effect of NG-R1 on A549 cell proliferation. The BeyoClick EdU-594 cell proliferation detection kit was used to assess the effect of NG-R1 on A549 cell proliferation. As shown in Fig. 2, treatment with 0.4 mg/ml NG-R1 significantly reduced the proliferation rate of A549 cells compared with that in the control group (P<0.01). Furthermore, the proliferation rate of A549 cells decreased progressively with increasing concentrations of NG-R1, indicating that NG-R1 significantly inhibited A549 cell proliferation in a dose-dependent manner (all P<0.01).

Effect of NG-R1 on A549 cell migration. The wound healing assay results demonstrated that the migration rates in the 0.4, 0.8 and 1.6 mg/ml NG-R1 treatment groups were significantly lower than those in the control group (all P<0.01; Fig. 3), indicating that NG-R1 effectively inhibited the migration of A549 cells.

Effect of NG-R1 on A549 cell invasion. Compared with that in the control group, the invasion rate of A549 cells was significantly reduced in a dose-dependent manner following 72 h of treatment with 0.4, 0.8 and 1.6 mg/ml NG-R1 (all P<0.01; Fig. 4), indicating that NG-R1 inhibited the invasive ability of A549 cells.

Effect of NG-R1 on the ROS levels of A549 cells. The fluorescent probe DCFH-DA was used to measure ROS levels in A549 cells following 72 h of treatment with various concentrations of NG-R1. As shown in Fig. 5, treatment with 0.4, 0.8 or 1.6 mg/ml NG-R1 significantly increased ROS levels in A549 cells (all P<0.01), which may indicate the induction of ferroptosis.

Effect of NG-R1 on the expression levels of ferroptosis-related proteins in A549 cells. As shown in Fig. 6, treatment with 0.4 mg/ml NG-R1 did not significantly alter TfR1 protein

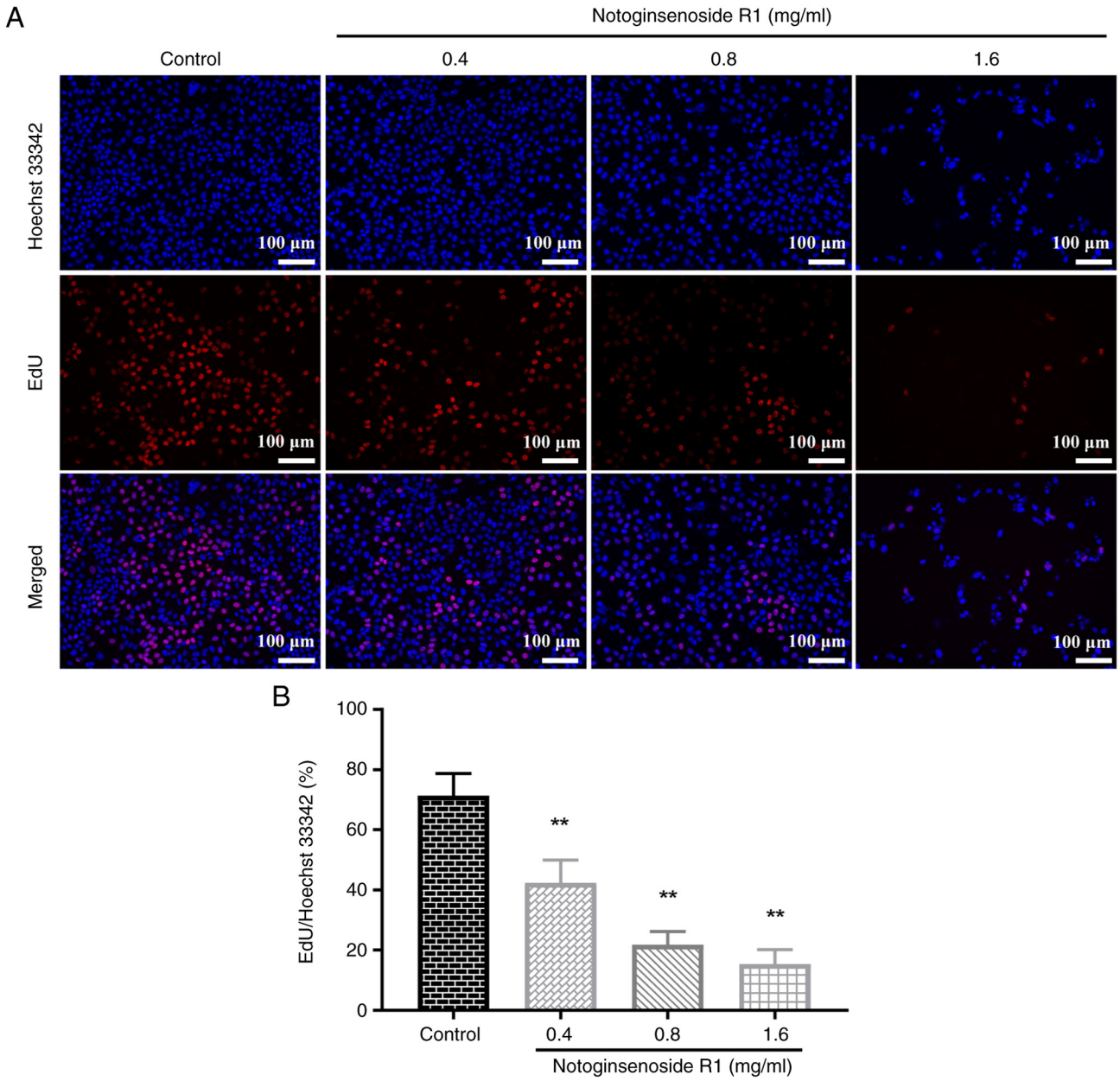

Figure 2. Effect of Notoginsenoside R1 on A549 cell proliferation (n=3). (A) Representative fluorescence micrographs of cell proliferation obtained by EdU assay. Top, Hoechst 33342 nuclear staining (blue); middle, EdU-labeled proliferating cells (red); bottom, merged image (Hoechst 33342 + EdU). Scale bar, 100 μm. (B) Proliferative ability of A549 cells in the EdU assay. Data are presented as the mean ± standard deviation. The one-way ANOVA result was $F(3, 8)$, 49.33. **P<0.01 vs. control group.

levels, whereas 0.8 and 1.6 mg/ml concentrations significantly increased TfR1 expression in A549 cells (all P<0.01). Additionally, NG-R1 treatment at concentrations of 0.4, 0.8 and 1.6 mg/ml significantly downregulated the protein expression levels of SLC7A11 (P<0.05, P<0.01), FTH1 (P<0.05 and P<0.01) and GPX4 (P<0.05 and P<0.01). These results suggested that NG-R1 may modulate ferroptosis-related proteins and induce ferroptosis in A549 cells.

Discussion

The present study is, to the best of our knowledge, the first to demonstrate that NG-R1 induces ferroptosis in human NSCLC A549 cells and to explore its underlying mechanisms. The results of the present study showed that NG-R1 significantly inhibited the viability, proliferation, migration and invasion of A549 cells in a dose-dependent manner. Notably, western blot analysis revealed that NG-R1 upregulated TfR1 while downregulating SLC7A11, GPX4 and FTH1, suggesting that its anticancer effects may have been mediated through ferroptosis in A549 cells (16).

The findings of the present study are consistent with those of previous studies demonstrating the anticancer effects of NG-R1 and its analogs, particularly against NSCLC (23,26). In a similar manner to established ferroptosis inducers such as erastin, NG-R1 promotes ferroptosis by elevating intracellular ROS levels (27). The pronounced inhibition of A549 cell proliferation, migration and

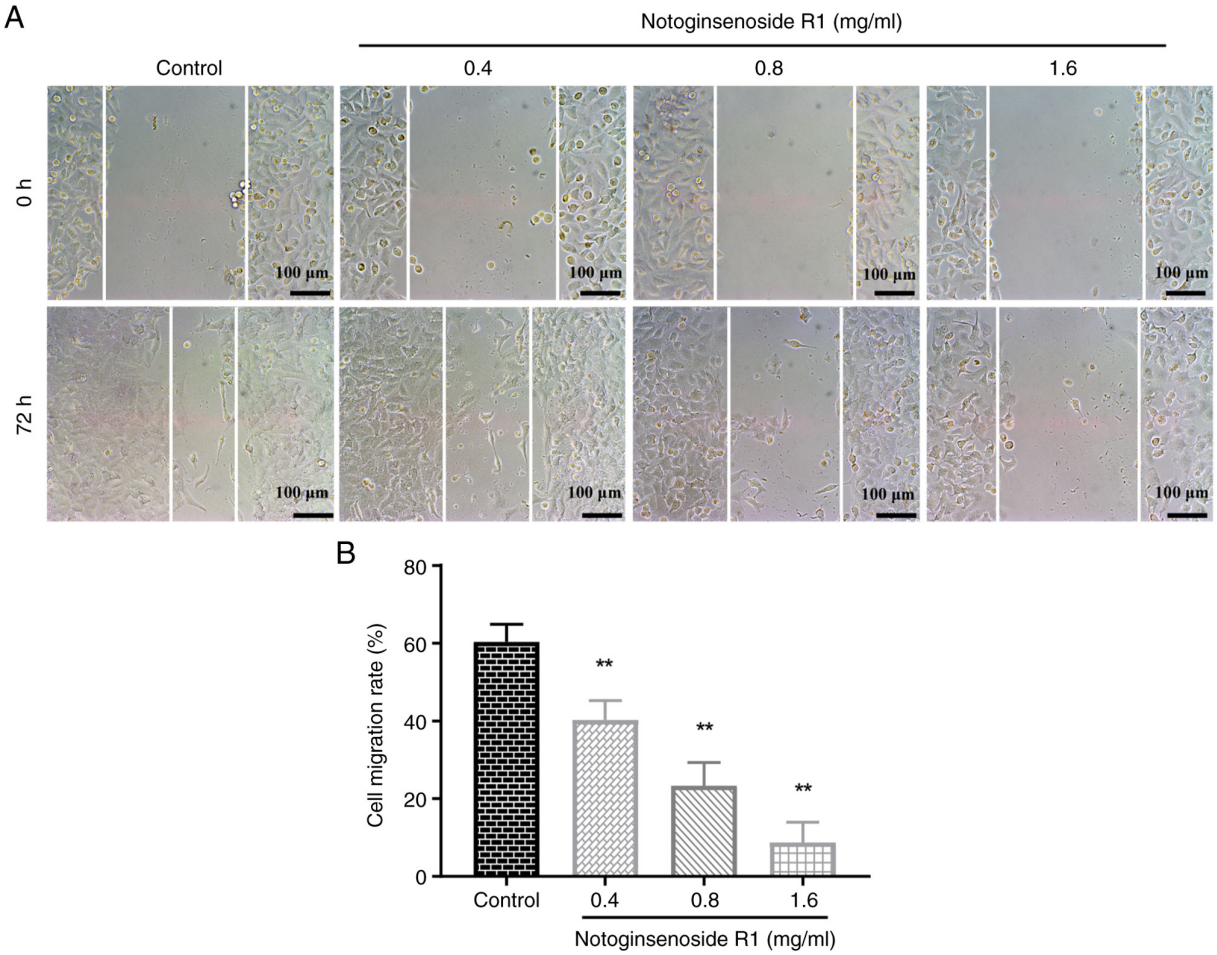

Figure 3. Effect of Notoginsenoside R1 on A549 cell migration (n=3). (A) Representative images of scratches at 0 and 72 h post-wounding (x100 magnification; scale bar, 100 μm). (B) Quantification of the wound-healing assay. Data are presented as the mean ± standard deviation. The one-way ANOVA result was F (3, 8), 55.43. and **P<0.01 vs. control group.

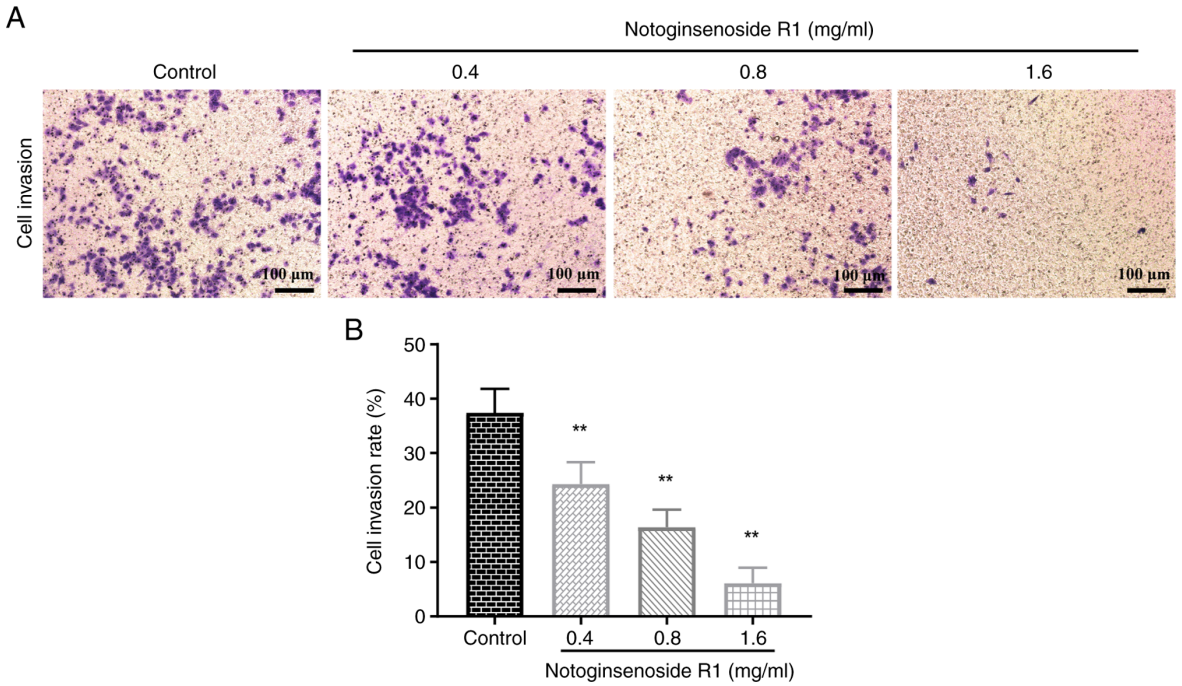

Figure 4. Effect of Notoginsenoside R1 on A549 cell invasion (n=3). (A) Representative inverted microscopy images of invasive cells (x100 magnification; scale bar, 100 μm). (B) Quantitative analysis of the Transwell invasion assay. Data are presented as the mean ± standard deviation. The one-way ANOVA result was F (3, 8), 38.55. **P<0.01 vs. control group.

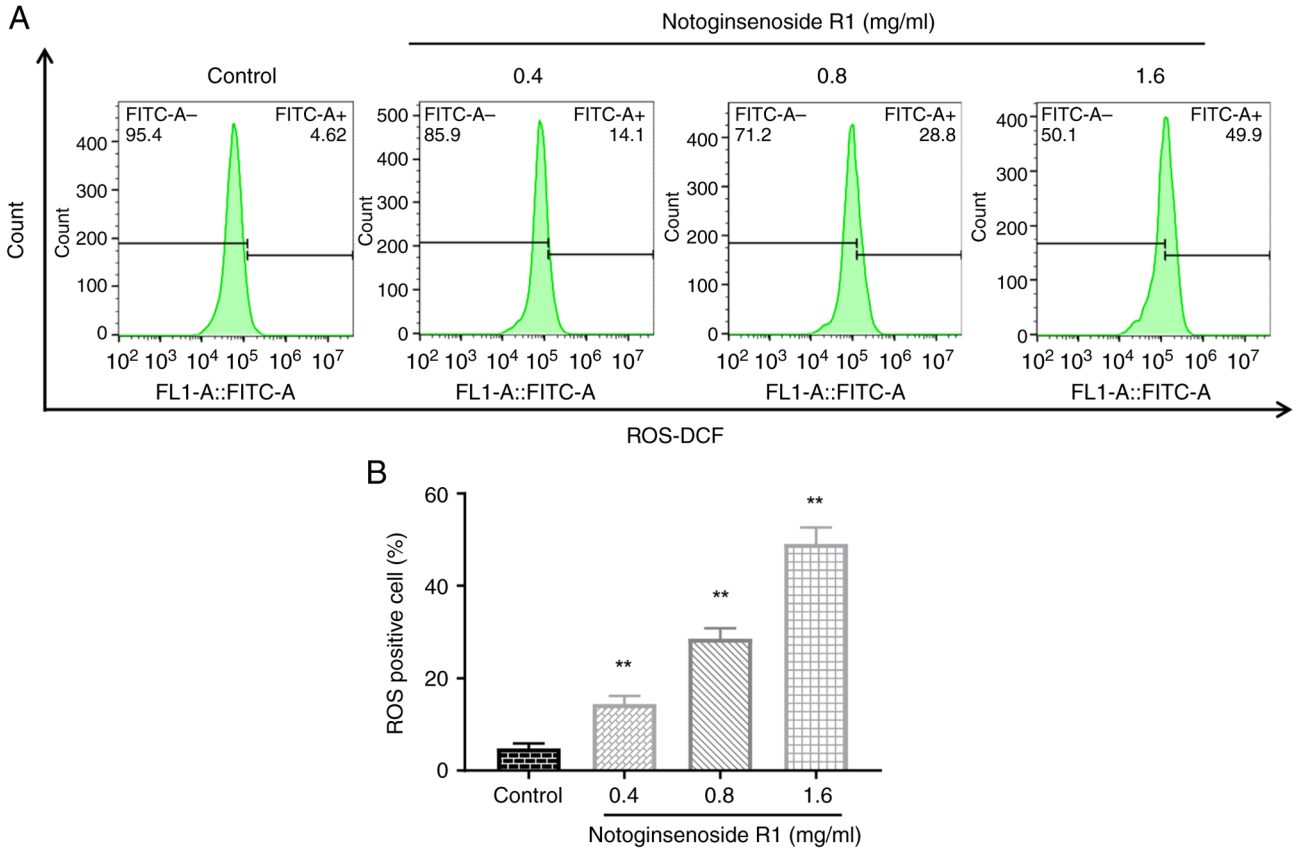

Figure 5. Effect of NG-R1 on ROS levels in A549 cells (n=3). (A) Flow cytometry plot of intracellular ROS levels using a 2',7'-dichlorofluorescein diacetate probe. (B) NG-R1 increased ROS levels in A549 cells in a dose-dependent manner. Data are presented as the mean ± standard deviation. The one-way ANOVA result was F (3, 8), 194.6. **P<0.01 vs. control group. DCF, dichlorofluorescein; NG-R1, Notoginsenoside R1; ROS, reactive oxygen species.

invasion observed in the present study further supports the potential of NG-R1 as an effective anticancer agent, providing new scientific evidence for its application in NSCLC treatment (23,26).

To further elucidate the molecular mechanisms underlying NG-R1-induced ferroptosis, the present study examined changes in the expression of key ferroptosis-related proteins. The results of the present study suggested that NG-R1 may regulate iron metabolism through multiple pathways, thereby activating ferroptosis, based on the findings from western blot analysis of related proteins. Notably, NG-R1 significantly downregulated SLC7A11, an important protein responsible for maintaining intracellular GSH levels and suppressing lipid peroxidation (27). SLC7A11 is commonly upregulated in NSCLC cells, contributing to tumor growth (19), and its downregulation by NG-R1 may reduce GSH synthesis, leading to increased lipid peroxidation and ferroptosis induction. The precise regulatory mechanism of NG-R1 on SLC7A11 warrants further investigation, potentially involving signaling pathways such as those mediated by nuclear factor erythroid 2-related factor 2 (Nrf2), p53 or other transcription factors (28,29). Additionally, NG-R1 significantly decreased the expression of GPX4, an important enzyme responsible for repairing lipid peroxides (21,27). This reduction may be secondary to GSH depletion following SLC7A11 downregulation, resulting in impaired GPX4 activity and the accumulation of toxic lipid peroxides, a hallmark of ferroptosis. Furthermore, NG-R1 could have modulated iron metabolism by significantly upregulating TfR1 and downregulating FTH1, thereby increasing the labile iron pool and promoting ferroptosis via enhanced Fenton reaction-mediated lipid peroxidation (13,27,30). Collectively, these findings suggest that NG-R1 induced ferroptosis in NSCLC cells by orchestrating the suppression of antioxidant defenses and dysregulation of iron homeostasis.

Although the present study provides evidence that NG-R1 induced ferroptosis in A549 cells, several important limitations remain. First, the lack of rescue experiments using ferroptosis-specific inhibitors, such as ferrostatin-1 or liproxstatin-1, and iron chelators such as deferoxamine, limits the suggestion that the observed cytotoxicity is primarily due to ferroptosis. Such experiments are important to exclude other forms of cell death, including apoptosis and necroptosis (27). Second, while alterations in key ferroptosis-related proteins were observed, the upstream regulatory mechanisms by which NG-R1 modulates proteins such as SLC7A11 and TfR1 remain ambiguous. Future investigations should focus on elucidating how NG-R1 influences these targets at the transcriptional and post-transcriptional levels, including the potential involvement of signaling pathways such as Nrf2, p53 and activating transcription factor 4 (28,29).

In conclusion, in the present study, NG-R1 was shown to inhibit the proliferation and migration of A549 cells, while

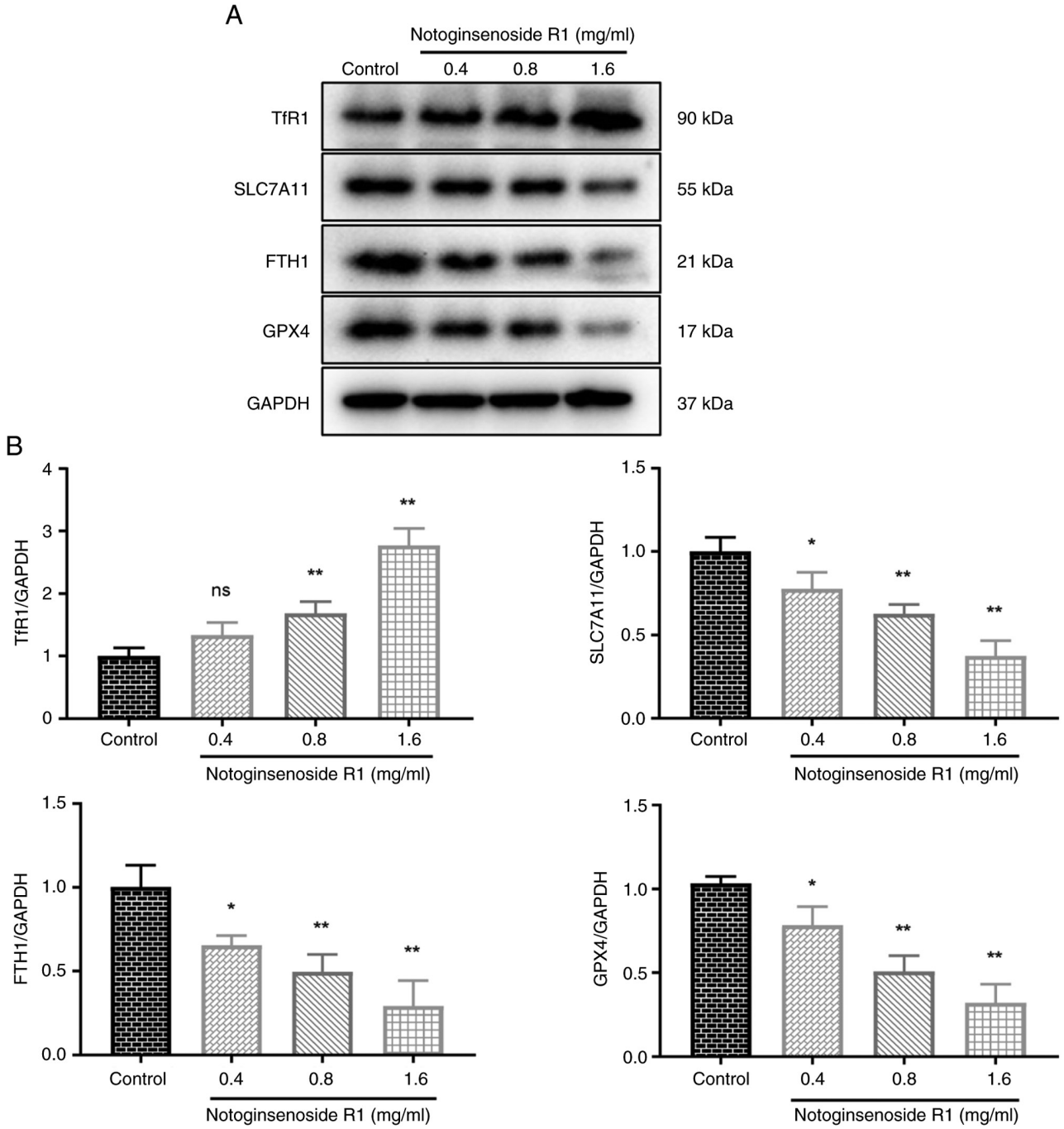

Figure 6. Effect of Notoginsenoside R1 on the expression levels of ferroptosis-related proteins (n=3). (A) Representative western blot images of the ferroptosis-related proteins. (B) Protein expression levels of TfR1, SLC7A11, FTH1 and GPX4 were examined by western blotting. Data are presented as the mean ± SD. The one-way ANOVA results were as follows: TfR1: F (3, 8), 41.41; SLC7A11: F (3, 8), 28.67; FTH1: F (3, 8), 19.68; GPX4: F (3, 8), 32.63. *P<0.05 and **P<0.01 vs. control group. FTH1, ferritin heavy chain 1; GPX4, glutathione peroxidase 4; ns, non-significant; SLC7A11, solute carrier family 7 member 11; TfR1, transferrin receptor 1.

significantly increasing intracellular ROS levels. Western blot analysis revealed that treatment with NG-R1 significantly upregulated TfR1 expression, and downregulated SLC7A11, GPX4 and FTH1 levels. These findings suggest that NG-R1 may induce ferroptosis in A549 cells and thus holds potential as an anti-lung cancer agent.

Acknowledgements

Not applicable.

Funding

The present work was supported by a grant from the Science and the Technology Plan Project of Yunnan Provincial Department of Science and Technology (grant no. 202101BA070001-267).

Availability of data and materials

The data generated in the present study may be requested from the corresponding author.

Authors' contributions

YZ was responsible for conceptualization, data curation, formal analysis, funding acquisition, investigation, methodology, project administration, resources, and writing, reviewing and editing the manuscript. ZM was responsible for data curation [data collection, cleaning (which involved data inspection and error correction: examining the collected raw data for recording errors, anomalies, or clearly illogical inputs) and validation], formal analysis, investigation, and writing, reviewing and editing the manuscript. YD was responsible for formal analysis, investigation and project administration. YZ and ZM confirm the authenticity of all the raw data. All authors read and approved the final manuscript.

Ethics approval and consent to participate

Not applicable.

Patient consent for publication

Not applicable.

Competing interests

The authors declare that they have no competing interests.

References

1. Dubey AK, Gupta U and Jain S: Epidemiology of lung cancer and approaches for its prediction: A systematic review and analysis. Chin J Cancer 35: 71, 2016.
2. Ferlay J, Colombet M, Soerjomataram I, Parkin DM, Piñeros M, Znaor A and Bray F: Cancer statistics for the year 2020: An overview. Int J Cancer 149: 778-789, 2021.
3. Jurisic V, Obradovic J, Nikolic N, Javorac J, Perin B and Milasin J: Analyses of $P16^{INK4a}$ gene promoter methylation relative to molecular, demographic and clinical parameters characteristics in non-small cell lung cancer patients: A pilot study. Mol Biol Rep 50: 971-979, 2023.
4. Petrović M, Bukumirić Z, Zdravković V, Mitrović S, Atkinson HD and Jurišić V: The prognostic significance of the circulating neuroendocrine markers chromogranin A, pro-gastrin-releasing peptide, and neuron-specific enolase in patients with small-cell lung cancer. Med Oncol 31: 823, 2014.
5. Socinski MA and Pennell NA: Best practices in treatment selection for patients with advanced NSCLC. Cancer Control 23 (4 Suppl): S2-S4, 2016.
6. Zappa C and Mousa SA: Non-small cell lung cancer: Current treatment and future advances. Transl Lung Cancer Res 5: 288-300, 2016.
7. Pilkington G, Boland A, Brown T, Oyee J, Bagust A and Dickson R: A systematic review of the clinical effectiveness of first-line chemotherapy for adult patients with locally advanced or metastatic non-small cell lung cancer. Thorax 70: 359-367, 2015.
8. Luo YH, Wang C, Xu WT, Zhang Y, Zhang T, Xue H, Li YN, Fu ZR, Wang Y and Jin CH: 18β-Glycyrrhetinic acid Has Anti-cancer effects via inducing apoptosis and G2/M cell cycle arrest, and inhibiting migration of A549 lung cancer cells. Onco Targets Ther 14: 5131-5144, 2021.
9. Proneth B and Conrad M: Ferroptosis and necroinflammation, a yet poorly explored link. Cell Death Differ 26: 14-24, 2019.
10. Galluzzi L, Vitale I, Aaronson SA, Abrams JM, Adam D, Agostinis P, Alnemri ES, Altucci L, Amelio I, Andrews DW, *et al*: Molecular mechanisms of cell death: Recommendations of the Nomenclature Committee on Cell Death 2018. Cell Death Differ 25: 486-541, 2018.
11. Hassannia B, Vandenabeele P and Berghe TV: Targeting ferroptosis to iron out cancer. Cancer Cell 35: 830-849, 2019.
12. Liang C, Zhang X, Yang M and Dong X: Recent progress in ferroptosis inducers for cancer therapy. Adv Mater 31: 1904197, 2019.
13. Bebber CM, Müller F, Clemente LP, Weber J and Karstedt SV: Ferroptosis in cancer cell biology. Cancers 12: 164, 2020.
14. Lewerenz J, Hewett SJ, Huang Y, Lambros M, Gout PW, Kalivas PW, Massie A, Smolders I, Methner A, Pergande M, *et al*: The Cystine/glutamate Antiporter system x(c)(-) in health and disease: From molecular mechanisms to novel therapeutic opportunities. Antioxid Redox Signal 18: 522-555, 2013.
15. Bridges RJ, Natale NR and Patel SA: System xc^- Cystine/glutamate antiporter: An update on molecular pharmacology and roles within the CNS. Br J Pharmacol 165: 20-34, 2012.
16. Dixon SJ, Lemberg KM, Lamprecht MR, Skouta R, Zaitsev EM, Gleason CE, Patel DN, Bauer AJ, Cantley AM, Yang WS, *et al*: Ferroptosis: An Iron-dependent form of nonapoptotic cell death. Cell 149: 1060-1072, 2012.
17. Yang WS, SriRamaratnam R, Welsch ME, Shimada K, Skouta R, Viswanathan VS, Cheah JH, Clemons PA, Shamji AF, Clish CB, *et al*: Regulation of ferroptotic cancer cell death by GPX4. Cell 156: 317-331, 2014.
18. Ursini F, Maiorino M, Valente M, Ferri L and Gregolin C: Purification from pig liver of a protein which protects liposomes and biomembranes from peroxidative degradation and exhibits glutathione peroxidase activity on phosphatidylcholine hydroperoxides. Biochim Biophys Acta 710: 197-211, 1982.
19. Ji X, Qian J, Rahman SMJ, Siska PJ, Zou Y, Harris BK, Hoeksema MD, Trenary IA, Heidi C, Eisenberg R, *et al*: xCT (SLC7A11)-mediated metabolic reprogramming promotes non-small cell lung cancer progression. Oncogene 37: 5007-5019, 2018.
20. Koppula P, Zhang Y, Zhuang L and Gan B: Amino acid transporter SLC7A11/xCT at the crossroads of regulating redox homeostasis and nutrient dependency of cancer. Cancer Commun (Lond) 38: 12, 2018.
21. Sun B, Xiao J, Sun XB and Wu Y: Notoginsenoside R1 attenuates cardiac dysfunction in endotoxemic mice: An insight into oestrogen receptor activation and PI3K/Akt signalling. British J Pharmacology 168: 1758-1770, 2013.
22. Guo Q, Li P, Wang Z, Cheng Y, Wu H, Yang B, Du S and Lu Y: Brain distribution pharmacokinetics and integrated pharmacokinetics of Panax Notoginsenoside R1, Ginsenosides Rg1, Rb1, Re and Rd in rats after intranasal administration of *Panax Notoginseng* Saponins assessed by UPLC/MS/MS. J Chromatogr B Analyt Technol Biomed Life Sci 969: 264-271, 2014.
23. Lee CY, Hsieh SL, Hsieh S, Tsai CC, Hsieh LC, Kuo YH and Wu CC: Inhibition of human colorectal cancer metastasis by notoginsenoside R1, an important compound from *Panax notoginseng*. Oncol Rep 37: 399-407, 2017.
24. Zhang W, Shu H, Fang L, Tang N, Li Y, Guo B and Meng F: Cancer inhibition mechanism of lung cancer mouse model based on dye trace method. Saudi J Biol Sci 27: 1155-1162, 2020.
25. Hsieh SL, Hsieh S, Kuo YH, Wang JJ, Wang JC and Wu CC: Effects of *Panax notoginseng* on the metastasis of human colorectal cancer cells. Am J Chin Med 44: 851-870, 2016.
26. Zhou Y, Zhang X, Wang X, Li Y, Liu Z, Zhang J, Chen L, Xu Y, Yang Y and Wang Z: Ferroptosis in cancer: From molecular mechanisms to therapeutic applications. Nat Rev Cancer 24: 1-15, 2024.
27. Xie Y, Hou W, Song X, Yu Y, Huang J, Sun X, Kang R and Tang D: Ferroptosis: Process and function. Cell Death Differ 23: 369-79, 2016.
28. Muckenthaler MU, Galy B and Hentze MW: Systemic iron homeostasis and the iron-responsive element/iron-regulatory protein (IRE/IRP) regulatory network. Annu Rev Nutr 28: 197-213, 2008.
29. Yang WS and Stockwell BR: Synthetic lethal screening identifies compounds activating iron-dependent, nonapoptotic cell death in oncogenic-RAS-harboring cancer cells. Chem Biol 15: 234-245, 2008.
30. Ganz T and Nemeth E: Hepcidin and iron homeostasis. Biochim Biophys Acta 1823: 1434-1443, 2012.